https://doi.org/10.1007/s41230-024-3102-1

Al-CeO_2-Mg refiner on grain refinement, cast fluidity and mechanical properties of AZ91 alloy

***Wen-xue Fan[1], Yu Bai[1, 2], **Hai Hao[1, 2], Bo Zhang[1, 3], Xing-guo Zhang[1, 2], and Kai-xi Jiang[2]**

1. Ningbo Research Institute of Dalian University of Technology, Ningbo 315016, China

2. Key Laboratory of Solidification Control and Digital Preparation Technology (Liaoning Province), School of Materials Science and Engineering, Dalian University of Technology, Dalian 116024, Liaoning, China

3. School of Energy and Power Engineering, Dalian University of Technology, Dalian 116024, Liaoning, China

Abstract: Grain refinement is a satisfying method to enhance the comprehensive performance of Mg alloys, and using grain refiners to improve the quality of Mg castings has become a common practice in the current casting industry. In this study, the effects of Al-CeO_2-Mg grain refiner addition on microstructure, cast fluidity, and mechanical properties of AZ91 alloy were systemically investigated by OM, SEM, DSC, TEM, sand Archimedean spiral mold fluidity test, and tensile test. The results show that the Al-CeO_2-Mg grain refiner has a remarkable effect on as-cast AZ91 alloy including notable grain refinement, enhancement of cast fluidity, and improvement of tensile properties. The average grain size of AZ91 alloy is refined by 63% with 1.0wt.% Al-CeO_2-Mg grain refiner. Meanwhile, the casting flow length of the as-cast AZ91 alloy is increased from 332 mm to 440 mm. The improvement of cast fluidity is attributed to the decreased liquidus temperature, shortening of solid-liquid two-phase temperature range, and refinement of microstructure.

Keywords: AZ91 magnesium alloy; grain refiner; cast fluidity; mechanical properties

CLC numbers: TG146.22 **Document code:** A

1 Introduction

As the lightest metal structural material, Mg alloy, with low cost, high specific strength/stiffness, and excellent electromagnetic shielding properties, has broad application prospects in automobile, aerospace, and electronic fields [1, 2]. Among them, AZ91 alloy, which has suitable ambient temperature mechanical properties, excellent casting performance, and high corrosion resistance, is one of the most widely used Mg alloys in approximately 90% of all Mg cast products [3, 4]. The fierce development of Mg alloy castings towards thin-walled and complexity requires excellent casting filling ability while ensuring satisfying mechanical properties, which puts forward higher requirements for mechanical properties and castability of AZ91 alloy [5].

***Wen-xue Fan**

Male, born in 1994, Ph. D. His research interests mainly focus on fine grain strengthening of magnesium alloys.

E-mail: fanwenxuedl@163.com

****Hai Hao**

E-mail: haohai@dlut.edu.cn

Received: 2023-08-28; Accepted: 2024-06-18

The literature review has revealed that the casting properties of alloys have a crucial relationship with their microstructure and solidification range [6, 7]. For instance, Kang and Sohn [8] found that an increase in the solidification range of Al-Cu-Si alloy resulted in a significant decrease in its fluidity. Fu et al. [9] also demonstrated that Ca and Sr alloying could refine the microstructure of Mg-Zn series alloys and enhance their casting fluidity, which deduced a lower defect propensity of casting alloy. The research conducted by Turen [10] revealed the addition of Sn with a content of about 0.5wt.% increased the fluidity length of AZ91 alloy resulting from the volume fraction reduction of shrinkage and the refinement of α-Mg grains and β-$Mg_{17}Al_{12}$ phases. Kwon and Lee [11] investigated the influence of grain refinement and oxide inclusions on the cast fluidity of Mg-Al alloy. The results showed that grain refinement significantly improved the fluidity. However, the oxide inclusions decreased fluidity due to the critical solid fraction stopping the flow depending on the amount of oxide inclusions in the flow channel.

Currently, grain refiner inoculation, the most commonly used melt treatment process in the foundry

industry, has become a common practice in the casting industry and has played an essential role in improving the casting performance of alloys [1, 12-15]. Davis et al. [16] have made some contributions to study the effect of Al-Ti-B grain refiner on the castability of AZ91alloy, and results showed that the grain refiner was observed to achieve a significant reduction in the grain size and hot tearing of AZ91D Mg alloy. Han et al. [15] reported the enhancement of fluidity and TiAl melt flow cessation mechanism by adding a TiB_2-containing grain refiner. They believed that the reduction of grain size of TiAl alloy was the virtual reason for the increased casting fluidity. However, limited work has been done to reveal the relevance of the grain refiner addition and casting fluidity of Mg alloys. The mechanism of microstructure refinement and changes in the solidification process resulting from grain refiner addition affected the casting fluidity of Mg alloys still needs to be determined.

Our previous research has prepared an Al-CeO_2-Mg grain refiner, and the grain refiner showed a satisfactory refinement effect on AZ31 alloy [17]. To investigate the impact of grain refiner addition on the microstructure and cast fluidity of AZ91 alloy, the Al-CeO_2-Mg grain refiner was selected as the inoculation in the present work. Therefore, the effects of Al-CeO_2-Mg grain refiner on the microstructure, mechanical properties, and cast fluidity of AZ91 alloy were studied, and the solidification behavior of the alloy with the Al-CeO_2-Mg grain refiner addition was also investigated in this study.

2 Experimental procedure

The grain refiner Al-CeO_2-Mg (Al-1.2Mg-0.9Ce-0.4O, wt.%) containing $MgAl_2O_4$ particles used for inoculation was prepared by a novel direct melt reaction (DMR) process. The refiner preparation process can be found in previous work [17]. The alloy used for the fluidity test was AZ91 alloy (Mg-8.9Al-1.0Zn-0.3Mn, wt.%). Pure Mg (purity 99.9wt.%), Al (purity 99.8wt.%), Zn (purity 99.9wt.%), and Mg-5Mn master alloy were provided as raw materials to fabricate AZ91 cast alloy. Firstly, pure Mg was melted at 730 °C, when it was completely melted, the impurities on the surface of the Mg melt were removed. Then, pre-weighed Al, Zn and Mg-5Mn master alloy were added to the 730 °C Mg melt, and the mixture was kept at 730 °C for 10 min. After the holding period, the melt was manually stirred under Ar atmosphere protection. Then, the pre-weighed 0.5wt.%, 1.0wt.%, 1.5wt.% and 2.0wt.% Al-CeO_2-Mg grain refiners were added to the AZ91 melt, respectively. Once the grain refiner was dissolved completely, the mixture melt was manually stirred to achieve a uniform distribution of the refining particles. Note that the grain refiner contains an Al element, which would affect the Al content in AZ91 alloy after the addition of grain refiner. Accordingly, the weight of pure Al used in AZ91 alloy casting was precisely adjusted to control the Al content in AZ91 alloy to be 8.9wt.% even after the addition of grain refiner. Finally, the AZ91 melt at 730 °C was poured into a concentric triple helix sand mold for testing the fluidity of AZ91 alloy. For comparison, AZ91 alloy without grain refiner was also prepared utilizing the same process. The sand mold for the fluidity test and the fluidity specimen is shown in Fig. 1. The fluidity spiral mold was precoated with boron-nitride solvent to prevent oxidative sticking and preheated in the atmosphere at 200 °C for 2 h. The flow length of the alloy was calculated by measuring the triple helix length and taking the average value. The manufacturing process and dimensions of the sand mold can be referred to the Refs. [9, 18]. In order to ensure consistency in composition and performance between the fluidity test samples and the tensile test samples, the remaining AZ91 melt after poured into the fluidity spiral mold was poured into a steel mold preheated at 200 °C (The steel mold for casting tensile test samples). This steel mold had dimensions with 50 mm in inner diameter, 140 mm in height, and 2 mm in wall thickness. Therefore, the size of the casting samples was a cylinder with a diameter of 50 mm and a height of 140 mm. Finally, three tensile specimens were taken out evenly in each casting.

The specimens for microstructure analysis were sectioned horizontally 10 mm from the bottom of the tensile specimen casting. The samples were kept for 24 hours at 410 °C and then quenched in water, and the sample after heat treatment was named homogenization samples. To more clearly observe the variation in grain size of AZ91 alloy, all as-cast specimens were homogenized by burying them in carbon powder to prevent oxidation of the specimens at high temperatures. The polished samples were etched with an acetic-picric acid solution for homogenization samples and a nitric acid-

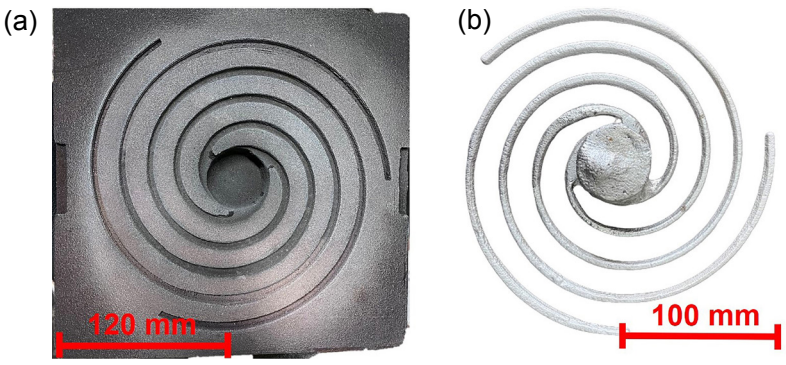

Fig. 1: Concentric triple helix sand mold (a) and fluidity specimen (b)

alcohol solution for as-cast samples. The average grain size of AZ91 alloys was measured by the linear intercept method (ASTM standard E112-10). An optical microscope (OM), a field emission scanning electron microscope (FESEM), and a high-resolution transmission electron microscope (HRTEM-JEM-2100F) were used for microstructure analysis. Room temperature tensile samples were machined according to the ISO 6892: 1998 standard. Figure 2 shows the dimensions of the standard tensile sample (unit: mm) and the schematic diagram of elongation (EL) calculation. The elongation of AZ91 alloy can be calculated by the equation: $EL = \frac{L_1 - L_0}{L_0} \times 100$. The room-temperature tensile tests were performed at a crosshead speed of 0.5 mm·min^{-1} on the universal testing machine (Instron-5982). These tensile tests were repeated twice to ensure the accuracy of the data.

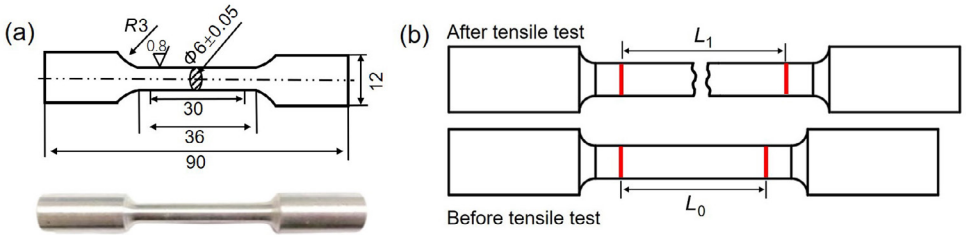

Fig. 2: Schematic diagram of dimensions of tensile samples (a) and elongation calculation (b) (unit: mm)

3 Results and discussion

Figure 3 shows the SEM microstructure and TEM images of the Al-CeO_2-Mg grain refiner. There are multilaterally shaped particles with a size of less than 2 μm and Ce-rich compounds larger than 10 μm distributing on the Al matrix, as shown in Fig. 3(a). The Ce-rich compounds are $Al_{11}Ce_3$ phases according to the energy spectrum analysis of Point I in the top right corner of Fig. 3(a). To observe the multilaterally shaped particles more clearly, TEM microstructure observation was performed. The TEM microstructure of multilaterally shaped particles in the Al matrix is shown in Fig. 3(b). Combine the EDS analysis, which illustrates the distribution of Al, Mg, and O elements in Region A [Figs. 3(c)–(f)] with the selected area electron diffraction (SAED) image of Point B [Fig. 3(g)] as shown in Fig. 3(b), it can be provisionally concluded that the multilaterally shaped particle is $MgAl_2O_4$. XRD pattern of the prepared Al-CeO_2-Mg grain refiner is shown in Fig. 4. $MgAl_2O_4$ and $Al_{11}Ce_3$ peaks are both detected in the grain refiner, which is consistent with the microstructure characterization results of the grain refiner. The high-resolution morphology of the Al matrix and the $MgAl_2O_4$ particle is shown in Fig. 3(h), and the inverse fast Fourier transform (IFFT) image of Region D in Fig. 3(h) proves that the particle on the left is $MgAl_2O_4$. A clean and tidy interface between the $MgAl_2O_4$ particle and the Al matrix is observed, indicating a good bonding relationship between the two phases. This demonstrates that the $MgAl_2O_4$ particles are produced by the in-situ reaction, which is consistent with our previous work [17].

The OM images and AGS variation of the AZ91 alloys are shown in Fig. 5. The average grain size (AGS) of AZ91 alloy decreases from 217 μm to 108 μm with the addition of 0.5wt.% Al-CeO_2-Mg grain refiner. When the addition amount of grain refiner is 1.0wt.%, the AZ91 alloy with the smallest AGS of 82 μm is obtained, indicating that 1.0wt.% is the optimal

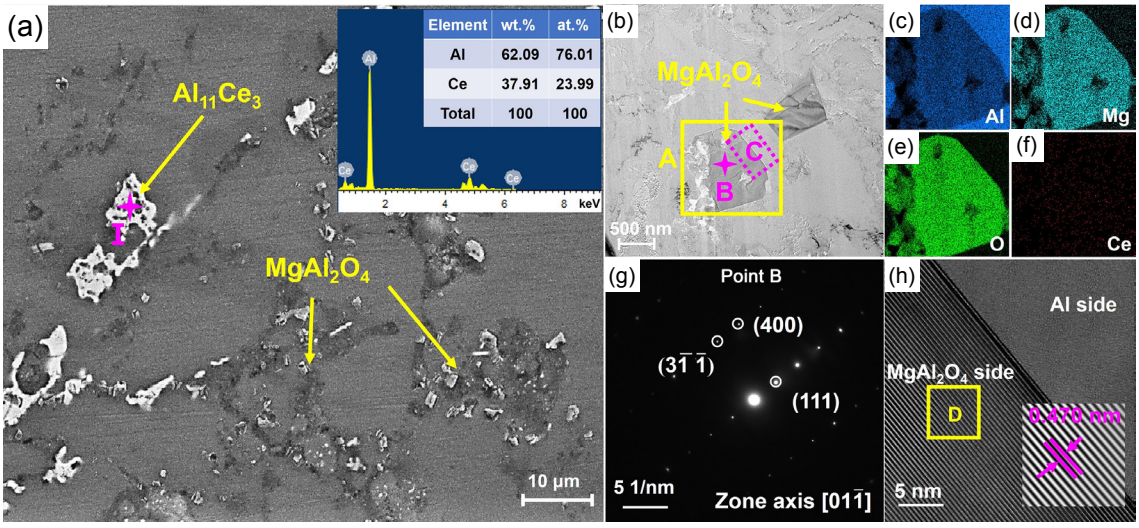

Fig. 3: (a) Microstructure of Al-CeO_2-Mg master alloy and EDS analysis of Point I; (b) TEM images of Al-CeO_2-Mg master alloys; (c)–(f) EDS analysis of yellow box in (b); (g) SAED image of Point B in (b); (h) HR-TEM image of interface C in (b) [Inverse Fourier Transform image of Region D in the lower right (h)]

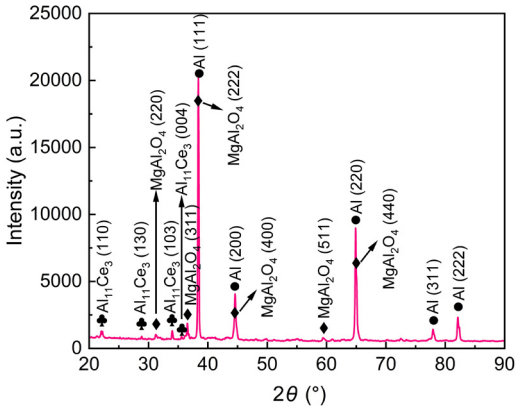

Fig. 4: XRD pattern of Al-CeO_2-Mg grain refiner

addition amount in this study. With the further increase of Al-CeO_2-Mg grain refiner to 1.5wt.% and 2.0wt.%, the grains of AZ91 alloys slightly coarsen, indicating that the refining effect of grain refiner is gradually weakened. However, the AGS of the refined AZ91 alloys is still significantly smaller than that of AZ91 alloy without grain refiner. The grain refining performance of Al-CeO_2-Mg is similar to that of Al-Ti-B [19], Al-Nb-B [20], or Al-Ti-C [21] refiner on Mg-Al alloys, which is called the "refinement saturation" phenomenon. Collision and aggregation occur in the AZ91 melt when an excessive number of particles are added. Ultimately, the effective refinement particles may settle and result in the reduction of effective nucleation sites, which is harmful to the effectiveness of grain refiners [21, 22].

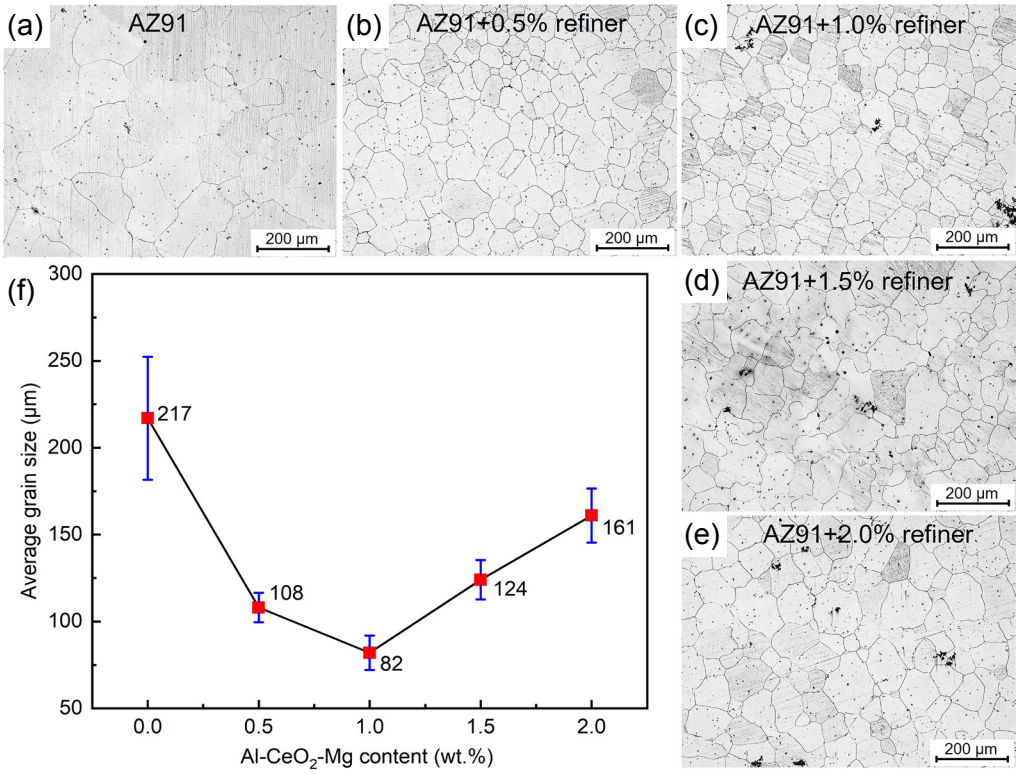

Fig. 5: OM images (a–e) and the variation of grain size (f) of AZ91 alloys with different amounts of Al-CeO_2-Mg grain refiner

The OM and SEM microstructures of as-cast AZ91 alloy with and without refinement are shown in Fig. 6. Some large-sized β-$Mg_{17}Al_{12}$ phases are distributed on the matrix of AZ91 alloy without grain refiner [Figs. 6(a)–(b)]. After 1.0wt.% Al-CeO_2-Mg grain refiner, the size of the β-$Mg_{17}Al_{12}$ phase becomes smaller, and the distribution becomes more dispersed compared with the un-refined AZ91 alloy, as shown in Figs. 6(c)–(d).

Efficient nucleation in the melt during the solidification process is fundamental for grain refinement of metallic materials [23, 24]. In this study, the $MgAl_2O_4$ particles and Ce-rich compounds in the Al-CeO_2-Mg grain refiner play critical roles in the refining effect of Mg alloy. Once the grain refiner enters the AZ91 melt, the $MgAl_2O_4$ particles can act as heterogeneous nucleation sites of α-Mg and promote massive nucleation in Mg melt, resulting in more grain boundaries and bringing about more dispersedly distributed β-$Mg_{17}Al_{12}$. The Ce element, as a rare earth element, has a large growth restriction factor in Mg and can restrain the growth of Mg grains [25]. The Ce atoms released from the Ce-rich compounds in the Al-CeO_2-Mg grain refiner tend to aggregate at the front of the solid-liquid interface, increasing the undercooling of the melt and inhibiting the growth of α-Mg grain [17]. In summary, both the heterogeneous nucleation of the $MgAl_2O_4$ particles and growth restriction effect of Ce elements' promote grain refining. It is worth noting that not all $MgAl_2O_4$ particles added in Mg melt can be activated to act as heterogeneous nucleation sites for α-Mg according to the free-growth model [26]. The $MgAl_2O_4$ particles which are not involved in Mg heterogeneous nucleation events can reduce the diffusion coefficient of

solute atoms and restrict the growth of primary grain which is called NP-induced growth control (NICG) theory [4]. These particles and solute manipulation effects impede the growth of Mg grains and the development of β-$Mg_{17}Al_{12}$ during the solidification process, resulting in fine-sized Mg and β-$Mg_{17}Al_{12}$ [20].

Good casting fluidity ensures that the Mg alloy has excellent mold-filling ability and effectively reduces the tendency of hot tears and the number of casting defects [13, 27]. The effects of Al-CeO_2-Mg grain refiner addition on the casting fluidity of AZ91 Mg alloy are shown in Fig. 7. Figure 7(a) shows the variation of flow length and grain size of AZ91 alloy with different amounts of Al-CeO_2-Mg grain refiner, and Fig. 7(b) shows the filling length and average grain size of the alloys with different amounts of grain refiner addition. The flow length of AZ91 alloy is improved after adding a grain refiner. Combined with the analysis of grain size variation of AZ91 alloy, it is found that the grain size is closely related to the casting fluidity of AZ91 alloy. Adding 0.5wt.% of Al-CeO_2-Mg grain refiner can enhance the flow length of AZ91 alloy from 332 mm to 393 mm. The casting fluidity of AZ91 alloy is optimal when the grain refiner addition is 1.0wt.%, and the flow length of AZ91 alloy improves to 440 mm, which increases by 33% compared to the un-refined AZ91 alloy. Combined with the analysis of Fig. 5 and Fig. 6, the improvement of casting fluidity is resulted from microstructure refinement, which is consistent with Fu and Han et al.'s research on Mg and TiAl alloys [9, 15].

Alloys with uniform and fine microstructure exhibit excellent casting fluidity [27, 28]. This is because the cast alloys with fine grain size cause the relatively delayed dendrite coherency time, which ensures that the melt can flow in the mold sufficiently before solidification, thus, achieving a significant increment of flow length. During the solidification process of

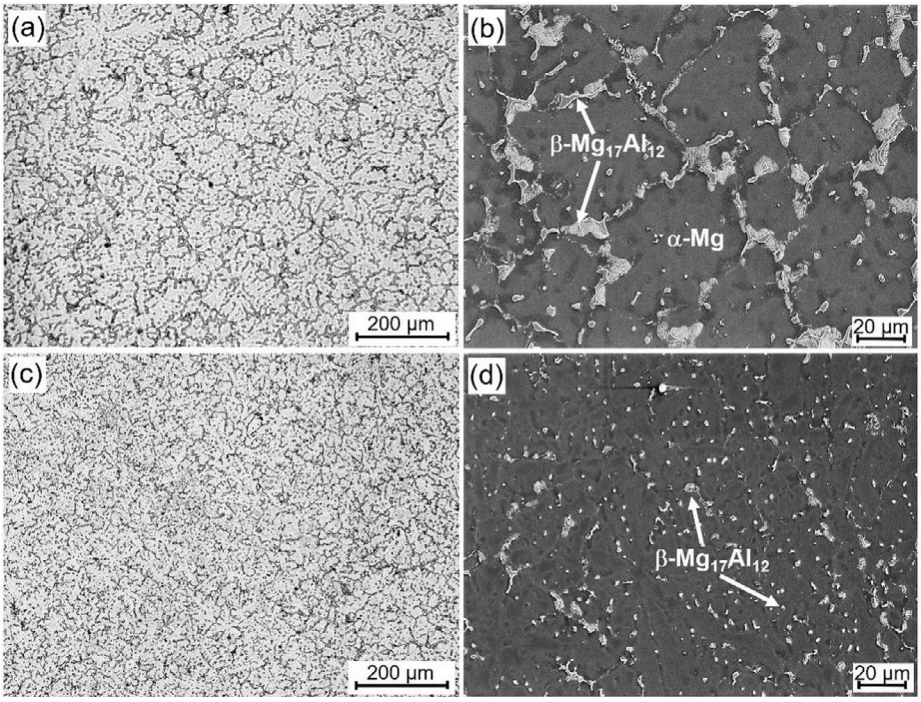

Fig. 6: OM and SEM images of as-cast AZ91 alloys: (a–b) AZ91 alloy; (c–d) AZ91 alloy with 1.0wt.% Al-CeO_2-Mg grain refiner

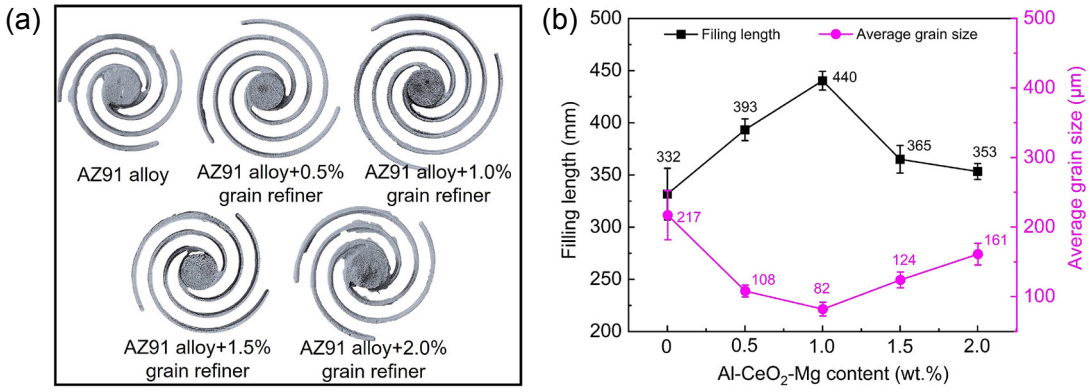

Fig. 7: Fluidity specimens (a), and filling length and average grain size variation (b) of AZ91 alloys with different amounts of Al-CeO_2-Mg grain refiner

Mg alloy, the primary grains would grow as dendrites. As the Mg dendrites grow, the tips of adjacent large-sized primary Mg dendrites encounter each other, and these contact points are the dendrite coherency points [29]. When the liquid metal flows along the spiral channel, once the temperature of melt drops to the liquidus temperature of Mg alloy, the molten metal starts to solidify. The primary dendrites produced in the Mg melt contact each other to create dendrite coherency points during the flow process, and the uncontacted parts will form reticulated voids. Subsequently, the molten metal will flow into the reticulated voids for replenishment, and finally, the melt stops flowing to form a solidified microstructure. Previous studies indicate that grain refiner can transform grain morphology from coarse dendrites to refined equiaxial grains during solidification, thus reducing the filling barrier of primary dendrites and improving the filling capacity of alloys [30, 31].

The schematic diagram of filling, flow, and solidification of AZ91 alloy with and without grain refiner in the Archimedean spiral mold is shown in Fig. 8. When the melt flows in the mold, several heterogeneous nucleate in the melt near the mold wall due to adequate nucleation undercooling and gradually grow up. At the same time, some heterogeneous nuclei also exists in the AZ91 melt, but the number of nuclei in the melt is small because of no grain refiner addition, as shown in Figs. 8(a)–(b). With the flow of the AZ91 melt, the number of nuclei gradually increases, and the size of the dendritic grains attached to the mold wall is also coarsen. The coarse dendritic grains become the filling obstacle of the melt and ultimately hinder the liquid metal's flow. The mechanism of melt flow stopping is that nucleated grains contact and connect at the front end of melt flow to form a dendrite coherency point, which greatly hinders the flow of the melt. The remaining liquid metal fills the gap near the dendrite coherency point, and the solidified microstructure is formed ultimately, as shown in Figs. 8(c)–(d).

After adding grain refiner, nucleation occurs in AZ91 melt due to the heterogeneous nucleation effect of $MgAl_2O_4$ particles, leading to the formation of refined grains. However, the growth of primary dendrites on the mold wall is hindered by refined grains, forming small columnar dendrites. The growth of primary dendrites formed on the mold wall is impeded by refined grains, eventually forming fine columnar dendrites [Figs. 8(e)–(f)]. These refined columnar grains growing on the mold walls are easily washed off by the liquid melt, and the process of the melt washing away the columnar grains increases the percentage of solids required to stop the flow of the melt, which further increases the flow time and length. In addition, the washed-away grains will re-enter the melt as heterogeneous nucleation sites, promoting microstructure refinement, as shown in Figs. 8(g)–(h).

The improvement of cast fluidity is also related to the modification of solidification behavior, which is resulted from grain refiner addition. Figure 9 shows the DSC curves of AZ91 alloy with and without Al-CeO_2-Mg grain refiner. The melting point of the AZ91 alloy with grain refiner during the heating process is 599 °C, which is lower than the 604 °C of the AZ91 alloy without refinement treatment. Similarly, the melting point of the refined AZ91 alloy during the cooling process (593 °C) is lower than that of the AZ91 alloy without adding the refiner (596 °C). The results in Fig. 9 show that adding grain refiner reduces the liquidus temperature (T_L) of the AZ91 alloy. Such similar conclusions about the decrease in the liquidus temperature of the melted alloy have also been found in other literature [32, 33].

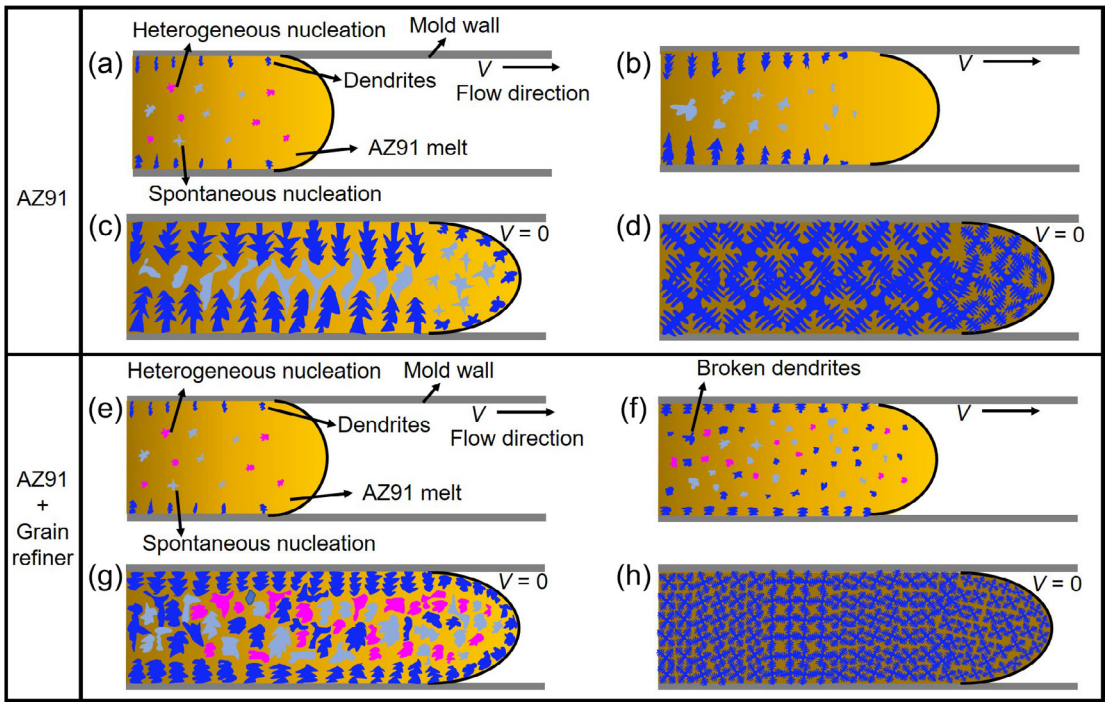

Fig. 8: Schematic diagram for flow-filling process of AZ91 melt in the mold without (a–d) and with (e–h) grain refiner addition

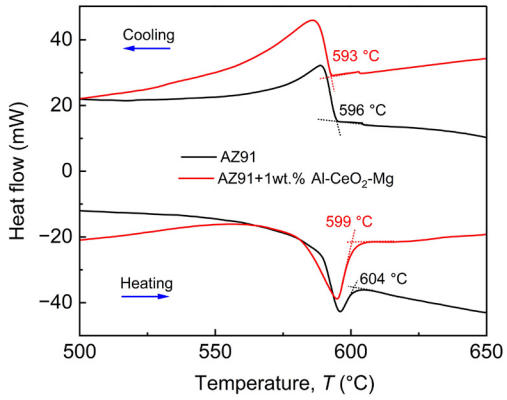

Fig. 9: DSC curves obtained from heating and cooling process for AZ91 alloy with and without Al-CeO_2-Mg grain refiner

The variation of the temperature range in the solid-liquid two-phase region can be related to the flow length of the alloy by the semiquantitative Flemings equation [34, 35]:

$$L = \mu\sqrt{2gH}\cdot(F\rho_l / p\alpha)\cdot\left\{\frac{f_s'\ \Delta H + c_l(T_p - T_{f_s'})}{T_l - T_m}\right\} \quad (1)$$

where L is the flow length of the liquid AZ91 alloy, μ is the flow consumption coefficient, H is the initial static pressure, ρ_l is the density of the liquid AZ91 alloy, F is the cross-sectional area of the Archimedean spiral mold runner, α is the heat transfer coefficient, p is the perimeter of the Archimedean spiral mold runner, f_s' denotes the fraction of solids at the tip of the liquid AZ91 alloy when the liquid stops flowing, ΔH and c_l are the latent heat of crystallization and specific heat of the liquid alloy, respectively, T_l is the liquid-phase line temperature, T_p is the pouring temperature, T_m is the temperature of the mold and $T_{f_s'}$ is the temperature at the time of stopping the flow of liquid alloy. According to Eq. (1), the factors affecting the flow length of AZ91 alloys include the physical properties of liquid Mg alloys, the mold condition, and the casting process. In addition, the research conducted by Malekan et al. [36] demonstrated that $T_{f_s'}$ can be defined as being T_{coh} (dendrite coherency point temperature). In this research, the AZ91 alloys used for fluidity testing has the same alloy composition, the casting process is under the same condition, and the fluidity molds are uniformly made using the sand Archimedean spiral mold. Therefore, parameters ρ_l, α, and ΔH in Eq. (1) are constants in the present study, then, Eq. (1) can be modified to the following equation:

$$L = \frac{[C_1 f_s' + C_2(T_p - T_{coh})]}{T_l - T_m} \quad (2)$$

where C_1 and C_2 are constants. In general, f_s' has a negligible effect on the flow length of the AZ91 alloy, so it is defined here as a constant. T_p and T_m are fixed values in the present study. Combined with the definitions of the above parameters, the flow length of AZ91 alloy is related to T_{coh} and T_l, and the flow length is inversely associated with T_{coh} and T_l. It can be concluded that the addition of refiner affects the solidification behavior of AZ91 alloy by lowering the liquid phase line temperature and narrowing the range of solid-liquid two-phase temperature according to the analysis of Fig. 9. The decrease in T_l can also delay the formation of the dendrite coherency point, thus lowering the T_{coh}. According to Eq. (2), the above changes in solidification behavior contribute to the increase of alloy fluidity.

The stress-strain curves, tensile properties, and fracture morphologies of AZ91 alloys with and without 1.0wt.% of Al-CeO_2-Mg grain refiner inoculation are shown in Fig. 10. The ultimate tensile strength (UTS) and elongation (EL) of the as-cast AZ91 alloy are increased from 146 MPa and 4.2% to 195 MPa and 7.2%, respectively, after addition of 1.0wt.% grain refiner. As shown in Figs. 10(c) and (d), the typical brittle fracture characteristics are observed in AZ91 alloy, which prove the poor plasticity. Some large cracks and tearing edges exist in fracture morphologies of AZ91 alloy without refinement attributed to the large-sized grains and brittle β-$Mg_{17}Al_{12}$ phases at its grain boundaries [Fig. 10(c)] [37]. Due to the brittle phases, cracks will preferentially sprout during the tensile process, leading to a decrease in the load-carrying capacity, thus resulting in weakening mechanical properties. Further observation on the microstructure in the vicinity of the fracture reveals that the fracture characteristics of the AZ91 alloy without refinement are an intergranular fracture, which further confirms the above observation. After adding the Al-CeO_2-Mg grain refiner, the size grains and β-$Mg_{17}Al_{12}$ phase distributed along grain boundaries in AZ91 alloy become uniformly fine [Fig. 10(d)]. The finely dispersed distribution of the β-$Mg_{17}Al_{12}$ phase reduces the probability of cracking during the tensile process, and the fine-grain effect also favors the tensile strength of the alloy. The changes in the morphologies and distributions of the β-$Mg_{17}Al_{12}$ phases effectively improve the bonding strength between the grains, so the crack extension will inevitably pass through the grains, forming a transgranular fracture [Fig. 10(d)].

4 Conclusions

The effects of Al-CeO_2-Mg grain refiner on the microstructure, cast fluidity, and mechanical properties of AZ91 alloy were investigated in this research. The conclusions are as follows:

(1) Adding 1.0wt.% Al-CeO_2-Mg grain refiner promotes the microstructure refinement of AZ91 alloy. The average grain size of AZ91 alloy is decreased from 217 μm to 82 μm. The size of β-$Mg_{17}Al_{12}$ phases in AZ91 alloy undergoes significant refinement, and their distribution becomes more dispersive and homogeneous after grain refiner addition.

(2) Adding an Al-CeO_2-Mg grain refiner effectively enhances the cast fluidity of AZ91 alloy. AZ91 alloy with 1.0wt.% Al-CeO_2-Mg grain refiner addition shows the optimal filling length of 440 mm, 33% higher than that of un-refined AZ91 alloy. The improvement of cast fluidity resulting from Al-CeO_2-Mg grain refiner addition is attributed to the decreased liquidus temperature and microstructure refinement.

(3) With 1.0wt.% Al-CeO_2-Mg grain refiner addition, the

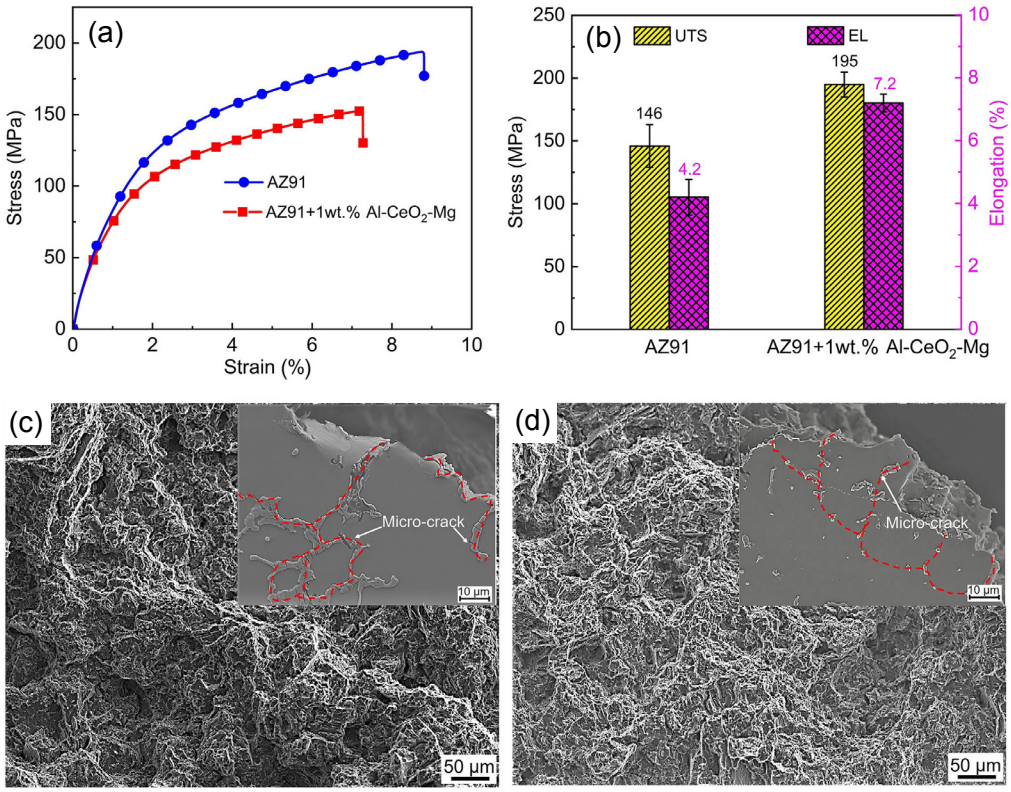

Fig. 10: Stress-strain curves (a) and mechanical properties (b) of AZ91 alloy with and without 1.0wt.% Al-CeO_2-Mg grain refiner, and fracture morphologies of AZ91 alloy without (c) and with (d) grain refiner

ultimate tensile strength and elongation of the as-cast AZ91 alloy were increased from 146 MPa and 4.2% to 195 MPa and 7.2%, respectively. Refinement of α-Mg grains and uniform distribution of β-$Mg_{17}Al_{12}$ phases are the key factors for the enhancement of strength and plasticity.

Acknowledgments

This work was supported by the National Natural Science Foundation of China (52171030) and the National Key Research and Development Program of China (2018YFA0702903).

Conflict of interest

Prof. Hai Hao is an EBM of *CHINA FOUNDRY*. He was not involved in the peer-review or handling of the manuscript. The authors have no other competing interests to disclose.

References

[1] Satya Prasad S V, Prasad S B, Verma K, et al. The role and significance of magnesium in modern day research–A review. Journal of Magnesium and Alloys, 2022, 10: 1–60.

[2] Wu H F, Hu W X, Ma S B, et al. Effect of Ce on microstructure and mechanical properties of Mg-Zn-Ce magnesium alloys. China Foundry, 2023, 20(4): 271–279.

[3] Wang Q D, Lu Y Z, Zeng X Q, et al. Study on the fluidity of AZ91+*x*RE magnesium alloy. Materials Science and Engineering: A, 1999, 271(1): 109–115.

[4] Li H N, Wang K, Xua G P, et al. Nanoparticle-induced growth behavior of primary α-Mg in AZ91 alloys. Materials & Design, 2020, 196: 109146.

[5] Weiler J P. Exploring the concept of castability in magnesium die-casting alloys. Journal of Magnesium and Alloys, 2021, 9(1): 102–111.

[6] Zhou Y, Mao P L, Wang Z, et al. Experimental investigation and simulation assessment on fluidity and hot tearing of Mg-Zn-Cu system alloys. Journal of Materials Processing Technology, 2021, 297: 117259.

[7] Dahle A K, Arnberg L. Development of strength in solidifying aluminum alloys. Acta Materialia, 1997, 45(2): 547–559.

[8] Kang B K, Sohn I. Effects of Cu and Si contents on the fluidity, hot tearing, and technical properties of Al-Cu-Si alloys. Metallurgical and Materials Transactions, 2018, 49: 5137–5145.

[9] Fu Y, Wang H, Zhang C, et al. Effects of minor Sr additions on the as-cast microstructure, fluidity and mechanical properties of Mg-4.2Zn-1.7RE-0.8Zr-0.2Ca (wt.%) alloy. Materials Science and Engineering: A, 2018, 723: 118–125.

[10] Turen Y. Effect of Sn addition on microstructure, mechanical and casting properties of AZ91 alloy. Materials & Design, 2013, 49: 1009–1015.

[11] Kwon Y D, Lee Z H. The effect of grain refining and oxide inclusion on the fluidity of Al-4.5Cu-0.6Mn and A356 alloys. Materials Science and Engineering: A, 2003, 360(1–2): 372–376.

[12] Ali Y, Qiu D, Jiang B, et al. Current research progress in grain refinement of cast magnesium alloys: A review article. Journal of Alloys and Compounds, 2015, 619: 639–651.

[13] Kimura R, Hatayama H, Shinozaki K, et al. Effect of grain refiner and grain size on the susceptibility of Al-Mg die casting alloy to cracking during solidification. Journal of Materials Processing Technology, 2009, 209(1): 210–219.

[14] Davis T A, Bichler L. Effect of Al-Ti master alloy on the grain refinement and hot tearing of AZ91 Mg alloys. Journal of Materials Engineering and Performance, 2023, 6(32): 2577–2586.
[15] Han J H, Liu Z D, Jia Y, et al. Effect of TiB_2 addition on microstructure and fluidity of cast TiAl alloy. Vacuum, 2020, 174: 109210.
[16] Davis T A, Bichler L. Novel fabrication of a TiB_2 grain refiner and its effect on reducing hot tearing in AZ91D magnesium alloy. Journal of Materials Engineering and Performance, 2018, 27(9): 4444–4452.
[17] Fan W X, Bai Y, Zuo G L, et al. Preparation of Al-CeO_2-Mg grain refiner for AZ31 Mg alloy via a novel direct melt reaction process. Materials Letters, 2022, 325: 132881.
[18] Fu Y, Wang H, Liu X T, et al. Effect of calcium addition on microstructure, casting fluidity and mechanical properties of Mg-Zn-Ce-Zr magnesium alloy. Journal of Rare Earths, 2017, 35(5): 503–509.
[19] Chen T J, Wang R Q, Ma Y, et al. Grain refinement of AZ91D magnesium alloy by Al-Ti-B master alloy and its effect on mechanical properties. Materials & Design, 2012, 34: 637–648.
[20] Fan W X, Bai Y, Zuo G L, et al. The control of NbB_2 particles in Al-NbB_2 master alloy and its effect on grain refinement of AZ91 magnesium alloy. Materials Science and Engineering: A, 2022, 854: 143808.
[21] Liu X T, Hao H. The influence of carbon content on Al-Ti-C master alloy prepared by the self-propagating high-temperature synthesis in melt method and its refining effect on AZ31 alloy. Journal of Alloys and Compounds, 2015, 623: 266–273.
[22] Fan W X, Bai Y, Zuo G L, et al. Enhanced grain refinement and mechanical properties of AZ91 alloy by a novel Al-5.1V-2.3B refiner containing VB_2 and VB particles. Materials & Design, 2023, 225: 111474.
[23] Fan Z Y, Gao F, Jiang B, et al. Impeding nucleation for more significant grain refinement. Scientific Reports, 2020, 10: 9448.
[24] Karakulak E. A review: Past, present and future of grain refining of magnesium castings. Journal of Magnesium and Alloys, 2019, 7(3): 355–369.
[25] Liu B S, Wu Z, Zhang Y Z, et al. Simultaneously enhanced the strength and ductility in $Mg_{17}Al_{12}$ intermetallic compound with Ce addition. Materials Letters, 2022, 320: 132324.
[26] Greer A L. Overview: Application of heterogeneous nucleation in grain-refining of metals. The Journal of Chemical Physics, 2016, 145(21): 211704.
[27] Ravi K R, Pillai R M, Amaranatha K R, et al. Fluidity of aluminum alloys and composites: A review. Journal of Alloys and Compounds, 2008, 456(1–2): 201–210.
[28] Dahle A K, Arnberg L. The effect of grain refinement on the fluidity of aluminum alloys. Materials Science Forum, 1996, 217–222: 259–264.
[29] Li P, Hou D H, Han E H, et al. Solidification of Mg-Zn-Zr alloys: Grain growth restriction, dendrite coherency and grain size. Acta Metallurgica Sinica (English Letters), 2020, 33(11): 1477–1486.
[30] Cui J, Luo T J, Li Y J, et al. Fluidity, microstructure, and tensile properties of sub-rapidly solidified Mg-6Al-4Zn-*x*Sn (*x*=0, 0.6, 1.2, 1.8) alloy. Acta Metallurgica Sinica (English Letters), 2021, 34(9): 1265–1276.
[31] Yang M B, Pan F S. Effects of Sn addition on as-cast microstructure, mechanical properties and casting fluidity of ZA84 magnesium alloy. Materials & Design, 2010, 31(1): 68–75.
[32] Fan W X, Bai Y, Li J H, et al. Grain refinement of Mg-Al alloys by a new Al-4.1V-1.7B refiner containing sole VB_2 particles. Journal of Materials Engineering and Performance, 2023, 32(2): 761–772.
[33] Xiao P, Gao Y M, Xu F X, et al. An investigation on grain refinement mechanism of TiB_2 particulate reinforced AZ91 composites and its effect on mechanical properties. Journal of Alloys and Compounds, 2019, 780: 237–244.
[34] Dahle A K, Karlsen S, Arnberg L. Effect of grain refinement on the fluidity of some binary Al-Cu and Al-Mg alloys. International Journal of Cast Metals Research, 1996, 9: 103–112.
[35] Flemings M C, Mollard F R, Taylor H F. Mould variables influence on fluidity of aluminum. AFS Transactions 1961, 69: 566–576.
[36] Malekan M, Shabestari S G. Effect of grain refinement on the dendrite coherency point during solidification of the A319 aluminum alloy. Metallurgical and Materials Transactions: A, 2009, 40(13): 3196–3203.
[37] Wang J J, Niu L, Zhang Y L, et al. Is $Mg_{17}Al_{12}$ ductile or brittle? A theoretical insight. Journal of Magnesium and Alloys, 2023, 11: 936–944.